Chemistry–A European Journal
Research Article
doi.org/10.1002/chem.202500626
Chemistry Europe
European Chemical Societies Publishing
www.chemeurj.org

Oxidation-Deformylation Cascade Catalyzed By a Mononuclear Copper Complex

Yongxing Wang,[a] Rogelio Gomez Pineiro,[a] Rébecca Leblay,[a] Michel Giorgi,[b] Sylvain Bertaina,[c] Maylis Orio,[a] Bruno Faure,[a] Marius Réglier,[a] and A. Jalila Simaan*[a]

In this study, two copper complexes were synthesized using N3 (arising from two pyridines and one amide group) containing ligands N-(2-picolyl)picolinamide (L^1H) and bis(2-pyridylcarbonyl)amine (L^2H), forming $[(L^1)Cu^{II}(OH_2)(NO_3)]$ (**1**) and $[(L^2)Cu^{II}(OH_2)_2](NO_3)$ (**2**). The reaction of complex **1** with hydrogen peroxide in alcoholic solvents yielded a formate-bound complex. Studies with isotopically labeled ^{13}C ethanol indicated that formate originates from the C1 of ethanol after C–C bond cleavage. Complex **1** was found to catalytically convert primary alcohols into formic acid probably following a two-step process: (i) alcohol oxidation to aldehyde and (ii) aldehyde deformylation. Further experiments with 2-phenylpropionaldehyde (2-PPA) confirm the ability of complex **1** to catalyze aldehyde deformylation. Both steps of the reaction are associated with significant kinetic deuterium isotope effects (KDIE), suggesting that hydrogen atom abstractions (HAA) occur during the rate-determining steps of both conversions. Overall, this system proposes a clean catalytic process for alcohol-to-formic acid conversion, operating under mild conditions, and offering potential synthetic applications.

Introduction

Selective oxidative transformations of organic substrates are of high importance in chemical and material synthesis to produce valuable products for chemical industry. To date, the majority of industrial oxidations are carried out using strong oxidants (*e.g.* nitric acid, potassium permanganate or chromium trioxide) in stoichiometric fashion, causing environmental issues. The use of clean oxidants such as molecular oxygen or hydrogen peroxide, that do not generate wasteful byproducts, is therefore a very attractive strategy to perform oxidation reactions.

Several metalloenzymes are able to perform selective oxidative transformations using dioxygen or hydrogen peroxide, under mild conditions and using abundant transition metal ions such as iron or copper.[1–4] In particular, copper metalloenzymes catalyze oxidation reactions using active sites with various topologies that have been a source of inspiration to develop bioinspired copper complexes.[5–10] The latter served both as tools to better understand the reaction of dioxygen/H_2O_2 with copper centers and as strategy to develop bioinspired catalysts.[11–14] Over the past decades, several mononuclear copper/oxygen species have been prepared and characterized to better unravel the reactivity of the species formed upon reaction of copper centers with dioxygen or hydrogen (alkyl) peroxide (Scheme 1).[6–9] Most detected intermediates exhibit electrophilic reactivity, mainly Oxygen Atom Transfer (OAT) or Hydrogen Atom Abstraction (HAA) from C–H, O–H or N–H bonds. Though, a few recent works have evidenced the nucleophilic reactivity of several copper/oxygen species such as η^1-Cu^{II}-superoxo,[15] Cu^{II}-alkylperoxo,[16] Cu^{II}-hydroperoxo[17] or dinuclear species.[18,19]

Aldehyde deformylation is a synthetically important oxidative C–C bond cleavage reaction that has become a representative reaction to probe the nucleophilicity of metal-oxygen species.[20,21] Although aldehyde deformylation generally involves nucleophilic attack of the metal-oxygen adduct to the carbonyl group of an aldehyde, several other mechanisms were discussed including electrophilic HAA steps.[20,22,23]

In the present work, we found that a mononuclear copper complex could catalyze the direct conversion of primary alcohols into formic acid probably following a two-step

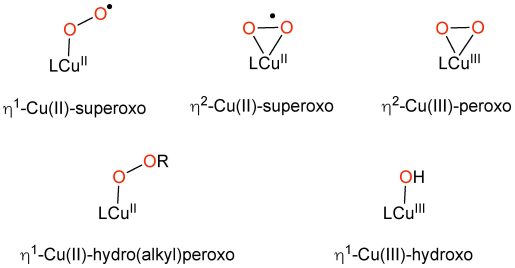

η^1-Cu(II)-superoxo η^2-Cu(II)-superoxo η^2-Cu(III)-peroxo

η^1-Cu(II)-hydro(alkyl)peroxo η^1-Cu(III)-hydroxo

Scheme 1. Selected mononuclear copper reactive species that were characterized and studied in the literature.

[a] *Dr. Y. Wang, Dr. R. Gomez Pineiro, Dr. R. Leblay, Dr. M. Orio, Dr. B. Faure, Dr. M. Réglier, Dr. A. Jalila Simaan*
Aix Marseille Univ, CNRS, Centrale Med, ISM2, Marseille, France
E-mail: Jalila.simaan@univ-amu.fr

[b] *Dr. M. Giorgi*
Aix Marseille Univ, CNRS, Centrale Med, FSCM, Marseille, France

[c] *Dr. S. Bertaina*
Aix Marseille Univ., CNRS, Université de Toulon, IM2NP, Marseille France
Marseille, France

Supporting information for this article is available on the WWW under https://doi.org/10.1002/chem.202500626

cascade consisting of *(1)* alcohol oxidation to aldehyde and *(2)* aldehyde deformylation generating formic acid or formate. We used the ligands *N*-(2-picolyl)picolinamide ($\mathbf{L^1}$H) and bis(2-pyridylcarbonyl)amine ($\mathbf{L^2}$H), to prepare the corresponding complexes [($\mathbf{L^1}$)Cu^{II}(OH_2)(NO_3)] (**1**), and [($\mathbf{L^2}$)Cu^{II}(OH_2)$_2$](NO_3) (**2**) (Scheme 2). The complexes were structurally characterized and their spectroscopic and electrochemical properties were measured in solution. After reaction with hydrogen peroxide in alcoholic solvents, a formate bound complex was crystallized. In attempts to better understand the oxidative events, isotopically-enriched ^{13}C ethanol was used and the results revealed that formate arises from C1 of ethanol after C–C bond cleavage. Further studies allowed to propose a two-steps cascade conversion of alcohols and various primary alcohols: (1) oxidation into aldehyde and (2) aldehyde deformylation reaction. Among the two complexes, **1** is the only one able to directly convert alcohols into formic acid. Both steps display important kinetic deuterium isotopic effects (KDIE) upon labelling of ethanol implying that HAA is involved in their rate determining steps. Different primary alcohols were converted into formic acid. Overall catalytic conversion of alcohols into formic acid, appears to be a clean transformation, occurring in oxidation-deformylation steps catalyzed by the same copper complex. Such transformation, which occurs without side products, could turn out to be of synthetic relevance.

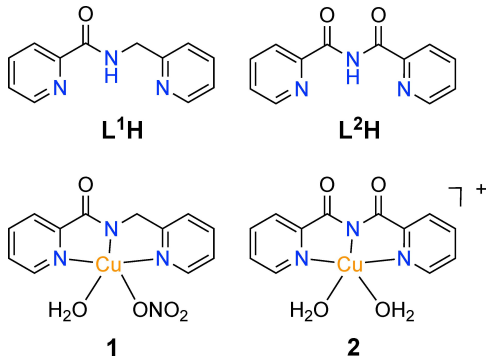

Scheme 2. Ligands and complexes used in this study.

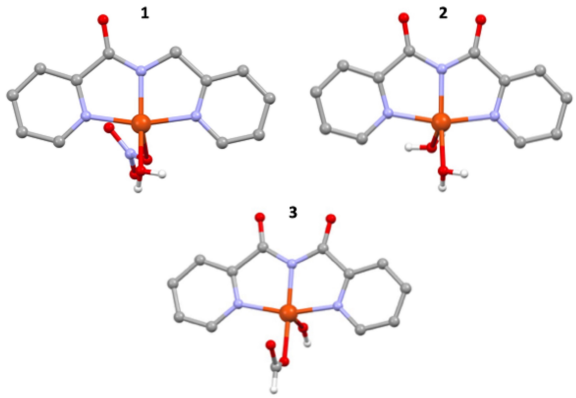

Figure 1. Representation of the crystallographic structures of **1**, **2** and **3** (counter ions were omitted for complex **2**). Hydrogen atoms were omitted for clarity except those on water, hydroxide or formate ligands.

Results and Discussion

Characterization of Complexes 1 and 2

The crystallographic structures of complexes **1** and **2**, obtained by Single Crystal X-ray Diffraction (SCXRD) are displayed on Figure 1 and selected crystallographic data and bond length/angles are reported in Tables S1&S3.

Visual inspection of complexes **1** and **2** reveals overall similar features with copper ions in distorted square-pyramidal geometries as supported by the angular structural parameters $\tau = 0.15$ and 0.09 respectively.[24] The geometry of the copper ions is further supported by analysis of the bond distances; the equatorial distances (3 N donors from the ligands and one O-atom from a water molecule) are in the range 1.9059(19)–2.0033(19) Å and are smaller that the elongated axial Cu–O distances (O from a nitrate counter ion or a water molecule) found in the range 2.2627(14) - 2.3131(19) Å (Table S3). Note that complex **1** crystallizes with a packing disorder (see Figure S1). Using a different MeOH/H_2O mixture for the crystallization conditions, we were also able to isolate crystals and solve the structure of [($\mathbf{L^2}$)Cu(CH_3OH)(NO_3)] (**2′**) that bears a methanol and a nitrate bound to the copper, consistent with the possibility to exchange solvent/counter-ion molecules on the copper center (Figure S2). Overall, these structures are very similar to those reported for similar copper complexes.[25–29]

In order to characterize the complexes in solution, X-band Electron Paramagnetic Resonance (EPR) spectra were recorded in frozen DMF, and the spin Hamiltonian parameters were extracted by simulation (Figure 2, Table S5). The EPR parameters are consistent with Cu(II) ions in distorted square-pyramidal geometries with the single electron in d_{x2-y2} orbital ($g_z > g_{x,y} > 2$).[30] EPR parameters are also consistent with [3N,1O] donors coordinated in the basal plane.[31,32] Addition-

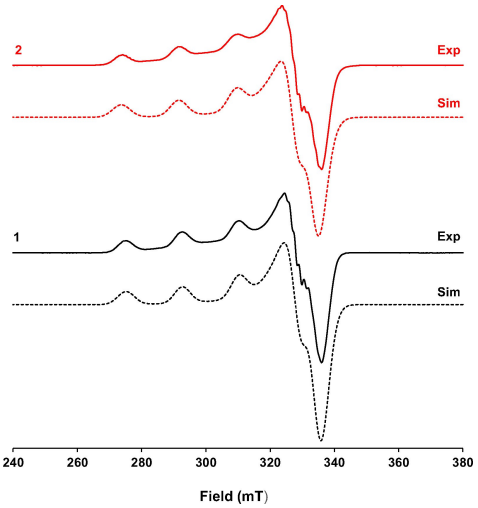

Figure 2. X-band EPR spectra of complexes **1** and **2** in DMF at 120 K. Plain lines correspond to experimental spectra (**1** = black, **2** = red). Dotted lines correspond to simulations. Main EPR parameters are **1**: $g_z = 2.233$; $A_z = 538$ MHz; $g_y = 2.056$; $g_x = 2.053$ and **2**: $g_z = 2.239$; $A_z = 550$ MHz; $g_y = 2.064$; $g_x = 2.058$.

ally, ^{14}N super-hyperfine pattern can be detected in the perpendicular regions and the mean magnitude of the splitting was determined graphically using the derivative of the signals (A^N = 40–43 MHz). The EPR spectra suggest that the main characteristics of the solid-state structures are maintained in solution.

Finally, cyclic voltammograms of the complexes were measured in DMF (Figure S6, Table S6). The complexes undergo a reduction process (E_{red}^1) at potentials around −0.9 V *vs.* Fc^+/Fc, which can be assigned to the reduction of Cu^{II} to Cu^{I}. In the case of **1**, a reoxidation peak can be more clearly detected at higher scan rates. Separation between the reduction and reoxidation peak is larger than the one expected for a reversible 1-electron process, which suggests that reorganization occurs upon reduction. When scanning towards high potentials, an anodic peak can be detected at 0.96 V in the case of complex **1**. This irreversible oxidation event can be associated to the generation of unstable formally Cu(III) complex.

Crystallization of Different Products Upon Reaction of 1 with H_2O_2 in EtOH

The addition of 10 equivalents of H_2O_2 and 2 equivalents of Et_3N on complex **1** placed in ethanol (or methanol) led to the isolation of several suitable crystals for SCXRD analysis (Scheme 3).

SCXRD analysis reveals that complex **3** is derived from complex **1** after several modifications (Figure 1, Tables S2 & S4). Firstly, the initial L^1 ligand is oxidized at the benzylic position to produce L^2. Secondly, a formate anion is found coordinated to the copper center in basal position and finally, a hydroxyl ligand is found in axial position. The resolution of the structure together with a careful analysis of the packing around the hydroxide ligand allowed to rule out the possibility of a second proton on the axial ligand and therefore of a bound water molecule instead of a hydroxide ligand. The copper would therefore be expected to be at the formally Cu(III) redox state. However, analysis of the crystal packing highlights the presence of channels of *ca.* 1 Å diameter that could accommodate labile protons to compensate the charge (Figure S3). In order to confirm the redox state of the copper in **3**, the single crystal was studied by EPR spectroscopy using a goniometer device (Figure S4). A classical Cu(II) EPR signature was obtained with well-defined g-tensor values of $g_x = 2.06$, $g_y = 2.08$ and $g_z = 2.24$ (Table S5). These values are very similar to those obtained for complexes **1** or **2** and suggest that the copper in **3** is in the Cu(II) redox state. Superconducting Quantum Interference Device (SQUID) measurements were also performed on the single crystal and the data confirm the presence of a S = 1/2 species, consistent with the Cu(II) redox state (Figure S4). Overall, these data support the description of **3** as the salt $[(L^2)Cu(OH)(HCOO)][H^+]$ constituted by negatively charged ions and mobile protons. The exact same complex **3** was also crystallized when the reaction was performed in methanol.

At least three other crystals were isolated from the reaction mixtures and allowed for the structural identification of the "mixture" **4**, as well as compounds **5a** and **5b**. The mixture **4** is a co-crystallization (packing disorder) of complexes **1** and **2** in a 2/3:1/3 mixture resulting in one carbonyl on the ligand displaying 100% occupancy and the other one 33% occupancy (Figure S2). Finally, the presence of **5a** and **5b** (already described in the literature)[33,34] is indicative of ligand degradation during the reaction.

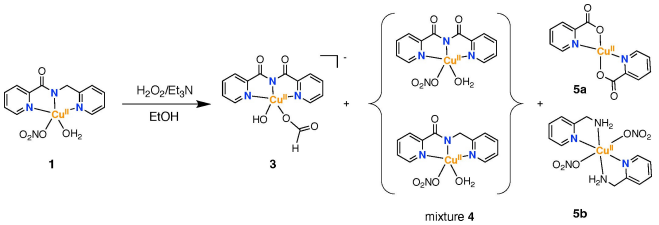

Scheme 3. Reaction of complex **1** with H_2O_2/Et_3N and structurally characterized complexes at the end of the reaction.

Investigation of Ethanol Conversion Into Formate

To quantify formic acid, we followed strategies that were developed for biological fluids.[35,36] The reactions were performed in sealed vials and concentrated sulfuric acid was added to quench the reaction and catalyze the conversion of formic acid into ethylformate that can be analyzed from the head-space gas by GC or GC-MS (Scheme 4A).

Origin of formate. The reaction was first performed using ^{13}C-labelled ethanol at the C1-carbon. Since ethanol is used for the derivatization of formic acid, one or two labelled ^{13}C atoms

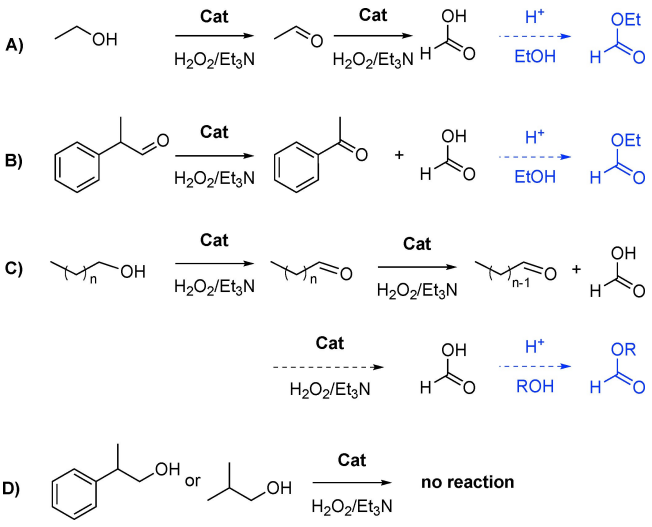

Scheme 4. A) Conversion of EtOH into formic acid in a two-step cascade including oxidation of EtOH into acetaldehyde and acetaldehyde deformylation B) 2-PPA deformylation C) oxidation of longer alcohols (n = 1,2) to lead to formate through possible successive cascades and D) other tested alcohols. H_2SO_4 is added at the end of the reaction to quench and upon addition of ethanol when relevant, convert formic acid into ethylformate that can be detected in GC.

can potentially be inserted in the ethylformate product. The reaction was performed using complex **1** and different amounts of labelled ethanol (from 18 to 53%). In all cases the observed mass distributions of ethylformate are in agreement with expected mass distributions considering that formate is formed from ethanol C1 carbon (Figure S7). These experiments support the fact ethanol is at the origin of formate (and ethylformate) and that formate arises from the C1 carbon of EtOH after C–C bond cleavage.

Comparison of the complexes. In order to further investigate the conversion of ethanol into formate, we quantified the production of formate from EtOH using DMF as solvent. The two complexes (as well as controls in absence of complex or using a copper salt) were placed in the presence of EtOH and the reaction was initiated by addition of H_2O_2/Et_3N. After 3 hours of reaction, only complex **1** significantly transformed EtOH into formic acid (Figure S8, ≈17% yield and 7 TON). Interestingly, when comparing the quantity of ethanol consumed to that of formate produced for the same experiment, a ratio 2:1 is evidenced. Since two molecules of ethanol are necessary to produce formate and then ethylformate for GC analysis, this points to a 1:1 ratio for the ethanol-to-formate conversion. Notably, since complex **2** is inactive for this transformation, the oxidative modifications undergone by **1** under catalytic conditions probably limit the efficiency of the system. Finally, the degradation product **5a** is found slightly active for EtOH conversion.

*Influence of reaction conditions using complex **1**.* Formate production was found dependent on the amount of complex, hydrogen peroxide and ethanol and in a lesser manner to that of triethylamine (Figure S9). In absence of ethanol, hydrogen peroxide or complex **1**, no formate is detected. Notably, when too much hydrogen peroxide is used (more that 100 equiv. *vs.* complex) the production of formate drops. This observation is consistent with hydrogen peroxide disproportionation by reactive metal species, limiting substrate's oxidation efficiency.[37,38] It has to be noted that the ratio EtOH consumed:formate produced is ~2:1 in all tested conditions (1:1 when considering that one ethanol is used to derivatize formic acid post-reaction). Ethanol-to-formate conversion is therefore a rather clean reaction with no detectable by-products.

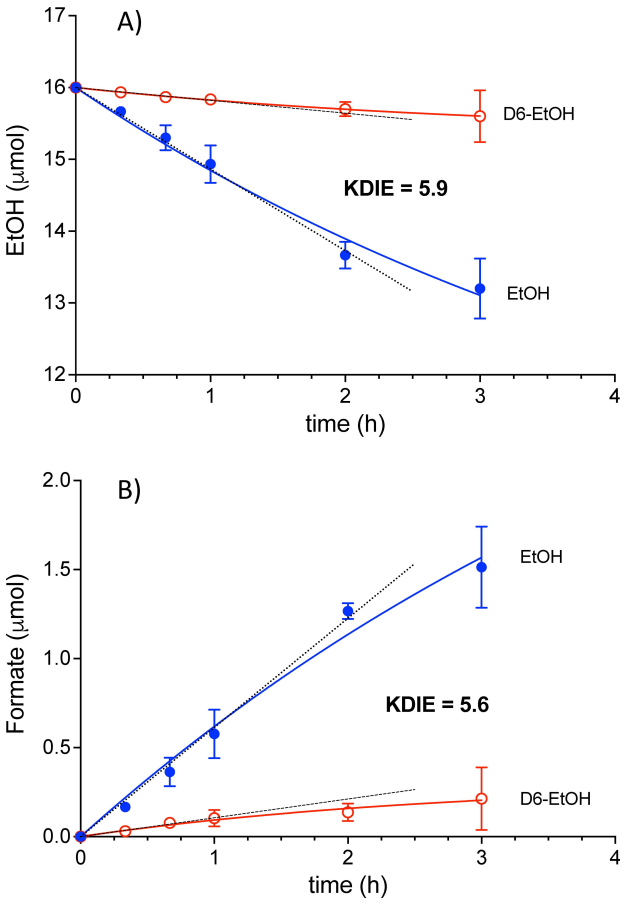

Figure 3. kinetics of the reaction of 1 in DMF with ethanol in the presence H_2O_2/Et_3N at 25 °C. (A) Consumption of EtOH (●) or D6-EtOH (○) as a function of reaction time and (B) production of formate from either EtOH (●) or D6-EtOH (○). Dashed lines represent the linear regression of the first points to extract initial rates. Kinetic Deuterium Isotope Effects were calculated using the ratio between initial rates (KDIE = v_H/v_D). Conditions: [1] = 2 mM, [H_2O_2] = 200 mM, [substrate] = 80 mM, [Et_3N] = 4 mM. Plain lines do not represent fits.

Kinetic Deuterium Isotopic Effect (KDIE). Both consumption of EtOH and production of formate were monitored with time (Figure 3). When deuterated ethanol (D6-EtOH) was used, ethanol consumption rate was slower than with unlabelled EtOH (Table 1). A significant KDIE can be determined by comparing the initial velocities ($KDIE_{EtOH}$ = 5.9), implying that a

Table 1. Substrates consumption and formate production rates[a] and calculated KDIE values. Rates were extracted using the linear part of the kinetic traces.[b]

Substrate	Substrate consumption rate	Formate production rate
EtOH	−1.06 µmol/min	0.56 µmol/min
D6-EtOH	−0.18 µmol/min	0.10 µmol/min
KDIE[b]	5.9	5.6
Acetaldehyde	−4.40 µmol/min	4.18 µmol/min
D4-acetaldehyde	−1.79 µmol/min	1.66 µmol/min
KDIE[b]	2.4	2.5

[a] Conditions: [1] = 2 mM, [H_2O_2] = 200 mM, [substrate] = 80 mM, [Et_3N] = 4 mM, 25 °C, DMF solvent; [b] determined using the ratio between the initial rates: KDIE = $V_{unlabelled}/V_{labelled}$.

HAA step is rate-limiting in the conversion of EtOH.[39] A similar high KDIE is measured for the appearance of formate ($KDIE_{form/EtOH} = 5.6$) strongly suggesting that HAA from EtOH is rate determining in ethanol-to-formate conversion. KDIE values are greater than the ones for HAA from similar substrates by hydroxyl radicals ($KDIE < 1.8$),[40,41] ruling out significant involvement of such radicals in the present transformation.

Hydroxyl radicals' production. Although KDIE value is not indicative of the presence of hydroxyl radicals, we evaluated the possible formation of such species using coumarin-3-carboxylic acid (CCA), a hydroxyl radical trap. CCA reacts with hydroxyl radicals and is converted into 7-hydroxy-CCA which displays fluorescence at 450 nm when excited at 390 nm.[42,43] The fluorescence detected is an indication of the amount of free hydroxyl radicals in solution. The fluorescence of 7-OH-CCA is proportional to the quantity of radicals that can reach the substrate. A part of produced hydroxyl radicals can react either with the solvent or with the organic ligands of the complexes. When placed in DMF in the presence of various quantity of hydrogen peroxide, no significant fluorescence signal could be detected, even when a copper salt was used as control. This is consistent with the fact that the solvent DMF acts as a radical scavenger. We therefore placed the complexes in aqueous solutions in the presence of CCA and hydrogen peroxide using our previously reported conditions.[13] Although the fluorescence increases in the case of free copper, the signals remain flat in presence of complexes **1** and **2** (Figure S12). This implies that almost no hydroxyl radicals reach the CCA probe and further supports the fact that diffusing hydroxyl radicals are not significantly involved here and that metal-centered species are responsible for HAA steps.

Mechanistic considerations. Direct oxidation of ethanol to formic acid involves C–C bond cleavage and probably an aldehyde as intermediate product. Oxidation of alcohols into the corresponding aldehydes or ketones using molecular copper-containing catalysts has been reported in the literature.[11,14,44–46] In most cases, copper-catalysts associated with redox active moieties (phenoxyl, TEMPO radical for instance) are used in the presence of molecular oxygen.[47–49] General mechanistic features involve a Cu^{II}-radical which can carry-out HAA of a bound alcohol/alkoxide substrate to yield the aldehyde and a Cu^{I} complex which subsequently reacts with dioxygen to regenerate the Cu^{II}-radical active species.[50,51] This mechanism is generally associated to KDIE typically ranging from 4–6, similar to the ones determined here. Some radical-free copper-based systems able to perform alcohol oxidation into the corresponding aldehyde were also reported.[45,46,52]

In line with literature, one can envision here that binding of the alcohol/alcoholate to the copper center occurs, weakening its α-C–H bond and facilitating HAA step.[53] Different copper/oxygen species could act as C–H abstraction species (Scheme 1). Attempts to isolate intermediates upon addition of hydrogen peroxide on **1** were unsuccessful. In the literature, mononuclear Cu(II)-OOH species have been identified upon reaction of hydrogen peroxide on copper(II) precursors.[6–9] Such Cu(II)-OOH entities could be the primarily C–H activating species in the present case. Since Cu(II)-OOH entities generally display low reactivity towards C–H bonds, it is also possible to propose the involvment of more oxidizing copper-oxyl entities (never observed in condensed phase so far).

Investigation of Deformylation Reactions.

Conversion of acetaldehyde. As mentioned above, oxidation of ethanol to formic acid involves C–C bond cleavage and probably an aldehyde as intermediate product. We thus evaluated the ability of the different complexes to convert acetaldehyde into formate. Quenching of the reaction by sulfuric acid was accompanied by the addition of ethanol to produce ethylformate. Again, complex **1** was found more efficient than **2** or copper salt (Figure S8). After 3 hours of reaction, *ca.* 8 mmol of acetaldehyde were consumed (≈50% conversion and 20 TON). The aldehyde-to-formate ratio was found close to 1:1 in all tested conditions, showing that conversion of aldehyde-to-formate is again a clean reaction without side products. Dioxygen dissolved in solution did not influence the efficiency of the system since experiments conducted under nitrogen did not significantly affect the yield and conversion. Formate production is found more than *7*-fold faster from acetaldehyde than from EtOH consistent with the fact that acetaldehyde does not accumulate when EtOH is converted to formate (Figure S10, Table 1). The use of deuterated acetaldehyde (D4) allowed the determination of isotopic effects $KDIE_{Acet} = 2.4$ and $KDIE_{form/acet} = 2.5$, suggesting that HAA is also rate-limiting in this transformation. KDIE values for HAA from aldehyde hydrogen or methyl hydrogen of acetaldehyde promoted by hydroxyl radicals were measured at 1.7 and 0.9 respectively.[54] The KDIE values measured here are higher than the ones reported for hydroxyl radicals therefore suggesting that metal-centered species are involved in the conversion of acetaldehyde to formate. Overall, these data are consistent with a clean conversion of ethanol into formic acid, in a two-steps cascade involving acetaldehyde as a non-detected intermediate product (Scheme 4A).

Reaction with 2-phenylpropionaldehyde (2-PPA). 2-phenylpropionaldehyde (2-PPA) is a classical substrate for probing aldehyde deformylation reaction (Scheme 4B). The reaction of 2-PPA with complex **1** in the presence of hydrogen peroxide/Et_3N allowed the detection of acetophenone and formic acid (Figure S11). This further confirms that complex **1** is able to catalyze aldehyde deformylation reaction.

Mechanistic considerations. Aldehyde deformylation has been evidenced using a variety of metal:dioxygen intermediates, including metal-(hydro)peroxo.[21–23] A widely accepted mechanism starts by an outer-sphere nucleophilic attack at the carbonyl atom leading to formic acid and deformylated products (e.g. alcohol, ketone, alkene).[22,23] Several alternative mechanisms have been discussed including mechanisms associated with C–H abstraction steps that are generally associated with significant KDIE values.[55,56] Such mechanisms can be relevant here based on our experimental KDIE. Overall,

our data indicate that addition of hydrogen peroxide to **1** generates copper-centered species able to perform challenging HAA from acetaldehyde ($BDE_{C\text{-}H}$ are ~89 or 95 kcal/mol).[57] Further work is in progress to better understand the mechanism of this transformations.

Substrate's Scope

Different other alcohols were then tested using **1** as catalyst to evaluate the scope of the reaction. Methanol is efficiently converted into formic acid (detected as methylformate) under those experimental conditions. When longer chain alcohols such as butanol or propanol, were used (Scheme 4C), 13% and 15% conversion were achieved respectively. Only one product was detected in GC after treatment with H_2SO_4. To probe the nature of this product, formic acid was added into the corresponding alcohols (propanol and butanol) and the products formed after sulfuric acid treatment were found to coincide with the ones obtained after reaction with **1** and are thus assigned to the corresponding formate esters. This underlines that complex **1** is able to perform the oxidative transformation of several primary alcohols, probably through aldehydes that are further deformylated. The smaller chain products are then probably oxidized leading to formic acid as the sole end-product.

When β-substituted alcohols were used (2-PPOH or isobutanol, Scheme 4D), no substrate consumption was observed indicating that complex **1** is not able to transform these alcohols. Since 2-PPA is efficiently deformylated by complex **1**, this suggests that the first step, *e.g.* alcohol oxidation into aldehyde, is critical with β-substituted alcohols. This is possibly due to steric hindrance which prevents the formation of copper-alcohol/alcoholate complex, and thus HAA step at β-position.

Conclusions

Complex **1** is able to catalytically transform alcohols into formic acid without side products, and under mild conditions. Labelling experiments using ^{13}C C1-labelled ethanol have indicated that formate arises from the C1 atom of ethanol, after C–C bond cleavage. This led us to propose a two-step cascade transformation: (1) oxidation of ethanol into acetaldehyde and (2) aldehyde deformylation with C–C bond cleavage. The ability of complex **1** to catalyze aldehyde deformylation was further demonstrated using acetaldehyde and 2-PPA as substrates. Both steps are associated with high KDIE values suggesting that hydrogen atom abstraction occurs during the rate-determining steps and that metal-centered species are involved. Finally several primary alcohols were successfully converted. Overall, our data are compatible with sequential conversion of primary alcohols into the corresponding aldehydes followed by deformylation, with no significant involvement of hydroxyl radicals. Alcohol oxidation into formic acid/formate appears as a "clean" transformation without significant generation of side products.

Formic acid is an important reagent in chemical industry finding various applications in the fields of leather tanning, textiles, or as a C1 building block for the synthesis of fine chemicals.[58,59] It is also a convenient liquid energy carrier (volumetric energy content of 2.1 kWh L^{-1}) and an interesting liquid H_2-storage molecule. Formic acid is currently mainly produced from fossil feedstocks. Ethanol is a renewable alcohol that can be produced from biomass and its direct conversion into formic acid could turn out to be of relevance for biobased chemicals production.

In addition, oxidation of alcohols has gained interest in the past decades for the development of Direct Alcohol Fuel Cells.[60–63] Most catalysts are based on Pt and Pd materials and efforts are directed towards the development of transition-metal based materials. So far, several problems limit the efficiency of the systems including sluggish kinetics, incomplete oxidation, catalyst poisoning, high material costs… In particular, the production of partially oxidized products, *e.g.* acetaldehyde and acetic acid, results from difficulties to break the C–C bond leading to efficiency loss. The reaction evidenced here, involving a simple copper catalyst and hydrogen peroxide, could therefore turn out to be of synthetic relevance both for biobased chemical industry and for energy production.

Experimental Section

Chemicals used in this work were purchased from Sigma-Aldrich with highest available purity and used without further purification. Solvents were purified using the solvent purification system Innovative Technology PS-MD-5. ^1H and ^{13}C NMR spectra were recorded on Bruker Avance III nanobay 300 MHz, 400 MHz or 500 MHz spectrometers. Chemical shifts are reported in ppm with the residual solvent signal as reference. Elemental Analysis were performed on Thermo Finnigan EA 11112 instrument. Two measurements were performed for each sample. UV-Visible absorption spectra were recorded on an Agilent Cary 60 spectrometer using 1 cm path-length quartz cuvettes. ESI-MS analyses were performed using a SYNAPT G2 HDMS (Waters) spectrometer equipped with a pneumatically assisted Atmospheric Pressure Ionization (API) source. The ion-spray voltage was 2.8 kV, the orifice lens was 20 V, and the nitrogen flux (nebulization) was 100 L h^{-1}. The HR mass spectra were obtained with a time-of-flight (TOF) analyser.

Synthesis of N-(2-picolyl)picolinamide (L^1H) ligand. The synthesis of the ligand was adapted from a previously described procedure.[25] To an anhydrous dichloromethane solution (9 mL) of picolinic acid (375 mg, 3.1 mmol), triethylamine (3.1 mmol, 308 mg), and 2-(aminomethyl)pyridine (3.1 mmol, 329 mg), phosphorous oxychloride (3.1 mmol, 467 mg) in dichloromethane (3 mL) was added dropwise with constant stirring at 0 °C. After a couple of minutes, an additional amount of triethylamine (6.1 mmol, 616 mg) was added. After 3 h, the reaction medium was neutralized with aqueous potassium bicarbonate. The organic layer was extracted and dried over $MgSO_4$. The solvent was evaporated yielding a viscous yellow residue (420 mg, 65%). ^1H NMR ($CDCl_3$; 500 MHz) δ in ppm: 8.93 (s, 1H), 8.66 (m, 2H), 8.22 (d, $J = 7.8$ Hz, 1H), 7.85 (td, $J = 7.7$, 1.7 Hz, 1H), 7.67 (td, $J = 7.7$, 1.8 Hz,

1H), 7.43 (ddd, $J = 7.5$, 4.8, 1.2 Hz, 1H), 7.35 (d, $J = 7.8$ Hz, 1H), 7.21 (dd, $J = 7.5$, 4.9 Hz, 1H), 4.85 (s, 1H). ^{13}C NMR (MeOD) δ in ppm: 167.1 (C=O), 159.1 (py), 151.1 (py), 150.0 (py), 138.9 (py), 127.9 (py), 123.9 (py), 123.3 (py), 123.0 (py), 45.5 (CH_2).

Synthesis of Bis(2-pyridylcarbonyl)amine ligand (L^2H). The synthesis of the ligand was adapted from a previously described procedure.[64] 2-picolinic acid (2 mmol, 246 mg) was mixed with 10 mL of $SOCl_2$ and the mixture was refluxed for 2 h. Then, the excess $SOCl_2$ was removed under vacuum. The resulting solid was redissolved in anhydrous toluene and 2-picolinamide (2 mmol, 240 mg) was added. The mixture was refluxed at 120 °C for 24 h. Aqueous potassium bicarbonate was then added and the organic layer was collected, washed with brine and dried over $MgSO_4$. The solvent was evaporated yielding a viscous yellow residue which was purified by chromatography using CH_2Cl_2/ethyl acetate 10:1 as the eluent to obtain **L^2H** (260 mg, 57%). 1H NMR (400 MHz, $CDCl_3$) δ in ppm: 13.04 (s, 1H), 8.76 (ddd, J = 4.8, 1.7, 0.9 Hz, 2H), 8.36 (dt, J = 7.9, 1.1 Hz, 2H), 7.94 (td, J = 7.7, 1.7 Hz, 2H), 7.56 (ddd, J = 7.6, 4.8, 1.2 Hz, 2H). ^{13}C NMR ($CDCl_3$) δ in ppm: 162.6 (C = 0), 149.2 (py), 148.6 (py), 137.7 (py), 127.5 (py), 123.4 (py).

Synthesis of the complexes. To a solution of ligand in methanol (0.5 mmol in 3 mL), a solution containing equimolar quantity of copper salt (copper nitrate trihydrate) in methanol (4 mL) was added dropwise under constant stirring. The reaction was left running with constant stirring at room temperature for 3 h. The initial light blue solutions turned dark blue and blue powders were collected by filtration after concentration of the solutions. Powders were resolubilized in MeOH/H_2O mixtures and suitable crystals for X-ray diffraction (XRD) were obtained by slow diffusion of Et_2O. $[(L^1)Cu(OH_2)](NO_3)$ (**1**): Elemental analysis: C 40.41 H 3.17 N 15.82; Calculated for $C_{12}H_{12}N_4O_5Cu$: C 40.51 H 3.40 N 15.75. UV-visible in DMF: λ/nm (ε/ M^{-1} cm^{-1}): 208 (3109), 628 (143). ESI-MS: m/z = 271 corresponding to $[(L^1)Cu]^+$ ion. $[(L^2)Cu(OH_2)](NO_3)$ (**2**): Elemental analysis: C 38.31 H 2.60 N 15.39; Calculated for $C_{12}H_{10}N_4O_6Cu$: C 38.98 H 2.73 N 15.15. UV-visible in DMF: λ/nm (ε/ M^{-1} cm^{-1}): 303 (3283), 640 (110). ESI-MS: m/z = 289 corresponding to $[(L^2)Cu]^+$ ion.

Reaction of 1 with H_2O_2 and Et_3N. Crystallization of 3, 4 and 5 a, 5 b. Reactions with H_2O_2 were performed in ethanol. Complex **1** was placed at 1 mM and 2 eq. of Et_3N and 20 eq. of H_2O_2 were added. After reaction the solutions were left to stand overnight at room temperature. Large blue crystals of **3** were collected. Small crystals of **5 a** and **5 b** were also present in some cases. Finally, the crystals were washed with DCM and the DCM fraction was left to evaporate leading to blue crystals of **4**.

Crystallographic structure determination. Suitable crystals were measured on a Rigaku Oxford Diffraction SuperNova diffractometer at different temperatures (Tables S1 & S2). Data collection reduction and multiscan ABSPACK correction were performed with CrysAlisPro (Rigaku Oxford Diffraction). The structures were solved using Olex2[65] by intrinsic phasing methods with SHELXT[66], and SHELXL[67] was used for full matrix least squares refinement. All H-atoms were found experimentally but re-introduced at geometrical positions and refined as riding atoms with their Uiso parameters constrainted to 1.5Ueq(parent atom) for the methyls and the oxygens, and to 1.2Ueq(parent atom) for the other carbons. The structures of **1** and **4** reveal packing disorders. The occupation factors for the oxygen atoms of the carbonyls in complex **1** and mixture **4** were first refined as free variables and then rounded and fixed at their final values. Relevant crystallographic data can be found in Tables S1 & S2. Crystal structure(s) have been deposited at the Cambridge Crystallographic Data Centre. Deposition Numbers: 2369676 (for **1**), 2370765 (for **2**), 2370764 (for **2′**) 2370747 (for **3**) and 2370741 (for **4**) contain the supplementary crystallographic data for this paper (https://www.ccdc.cam.ac.uk/services/structures?id=doi:10.1002/chem.202500626"). These data are provided free of charge by the joint Cambridge Crystallographic Data Centre and Fachinformationszentrum Karlsruhe (http://www.ccdc.cam.ac.uk/structures) Access Structures service.

EPR spectroscopy. Standard X-band, continuous-wave (cw) EPR spectra were recorded on frozen DMF solutions using ELEXSYS Bruker instrument equipped with BVT 3000 digital temperature controller. Typical parameters: temperature 120 K, microwave power: 10–20 mW, modulation frequency 100 kHz and intensity 3 G. Spectra simulations were performed using Matlab program package Easyspin.[68] Single crystal EPR measurements were performed using a conventional Bruker EMX spectrometer operating in X-band (f = 9.67 GHz). The spectrometer is equipped with an automatic goniometer. Since the crystallographic axes were not identified according to the morphology, the crystal was installed randomly on the sample holder. A series of spectra as function of the static field angle was recorded, then the crystal was rotated by 90° and a second series was recorded. The spectra were fitted using a derivative of a Lorentzian. The resonances fields as function of angle for the two series were fitted using Easyspin v6 in order to extract the principal value of the g tensor and the Euler in the morphology axes.

Superconducting quantum interface device (SQUID) measurements. Magnetic characterization has been performed using a conventional SQUID magnetometer MPMS-XL from Quantum Design working at a magnetic field up to 5 T and temperature down to 2 K. The samples (powder) are filled in polypropylene sleeves then sealed in order to remove the maximum of dioxygen, which give the signal around 50 K (antiferromagnetic transition). Magnetic contribution from the sample holder as well as diamagnetic contribution of the sample were removed.

Cyclic Voltammetry. Cyclic voltammetry measurements were performed with Biologic SP-150 potentiostat controlled with the EC-Lab software version 10.10. The experiments were conducted in 0.1 M nBu_4NPF_6 solutions (in DMF) using three-electrode configuration, with a glassy carbon electrode from Biologic with nominal radius = 0.2 cm as a working electrode, a Pt wire as auxiliary electrode, and a leakless AgCl/Ag reference electrode (eDAQ). Experiments were conducted in a 5 mL electrochemical cell equipped with an argon-purge system at room temperature. The redox potentials in the text are referred to Fc^+/Fc.

Catalytic assays. Typical catalytic oxidation assays were performed in 2 mL sealed vials, loaded with complex/Et_3N/H_2O_2/substrate in 1 mL reaction volumes kept at 298 K with a constant magnetic stirring. Different substrates were tested: ethanol, acetaldehyde, longer chain alcohols (propanol, butanol), 2-phenyl-1-propanol (2-PPOH), 2-phenylproprionaldehyde (2-PPA) and isobutanol. Concentrated sulfuric acid (25 μL) was added through the septum to the reaction mixture to stop the reaction. Formic acid was quantified following strategies that were developed for its quantification in biological fluids:[35,36] the addition of concentrated sulfuric acid in the presence of ethanol leads to the conversion of formic acid into ethylformate that can be quantified by GC. When acetaldehyde or 2-PPA were used as substrates, ethanol (40 equivalents *vs.* complex) was added, together with sulfuric acid, to allow conversion into ethylformate. Gas from the head-space (20 μL using a gas-tight syringe for GC-FID analysis) or solution mixtures (5 μL for GC-MS analysis) were injected into a Gas Chromatograph. Products were quantified by placing at least 5 different quantities of pure standards in the vial and subjecting

them to the same treatment before injecting the headspace or the liquid phase for GC analysis. GC-FID measurements were performed on a Shimadzu GC-14A equipped with Supelco Analytical fused silica capillary column (60 m×0.2 mm×0.5 μm film thickness). GC-MS analysis were performed using a Shimadzu GC-2010 plus equipment coupled with a Shimadzu GCMS-AP2010SE mass detector. The column installed was a Zebron phase ZB-5MS (60 m x 0.25 mm x 0.25 μm film thickness). Full details on methods and data are provided in SI (Tables S7–S11).

Hydroxyl radicals' detection. The assays were performed either in DMF or in 50 mM phosphate buffer at pH 8.5 using Coumarin-3-Carboxylic Acid (CCA) and following a previously reported procedure.[13] The fluorescence was monitored at 452 nm upon excitation at 395 nm using a BIOTEK Synergy MX microplate reader.

Acknowledgements

This work was supported by the French Agence Nationale de la Recherche (COSACH ANR-22-CE07-0032 & INSPIRE ANR-23-CE43-0012). Y.W. acknowledge The Chinese Scientific Council and R.L. acknowledge Region-Sud PACA for their Ph.D fellowships. The authors thank the CNRS research infrastructure INFRANALYTICS (FR 2054) for support. Finally, we are grateful to Dr. Cédric Colomban and Prof. Alexandre Martinez for interesting discussions.

Conflict of Interests

The authors declare no conflict of interest.

Data Availability Statement

The data that support the findings of this study are available in the supplementary material of this article.

Keywords: Copper · Alcohol oxidation · Deformylation · Catalysis · Bioinspired catalysis

[1] T. L. Poulos, *Chem. Rev.* **2014**, *114*, 3919–3962.
[2] B. Wang, X. Zhang, W. Fang, C. Rovira, S. Shaik, *Acc. Chem. Res.* **2022**, *55*, 2280–2290.
[3] C. E. Valdez, Q. A. Smith, M. R. Nechay, A. N. Alexandrova, *Acc. Chem. Res.* **2014**, *47*, 3110–3117.
[4] E. I. Solomon, D. E. Heppner, E. M. Johnston, J. W. Ginsbach, J. Cirera, M. Qayyum, M. T. Kieber-Emmons, C. H. Kjaergaard, R. G. Hadt, L. Tian, *Chem. Rev.* **2014**, *114*, 3659–3853.
[5] C. Citek, S. Herres-Pawlis, T. D. P. Stack, *Acc. Chem. Res.* **2015**, *48*, 2424–2433.
[6] S. Itoh, *Acc. Chem. Res.* **2015**, *48*, 2066–2074.
[7] C. E. Elwell, N. L. Gagnon, B. D. Neisen, D. Dhar, A. D. Spaeth, G. M. Yee, W. B. Tolman, *Chem. Rev.* **2017**, *117*, 2059–2107.
[8] B. Kim, K. D. Karlin, *Acc. Chem. Res.* **2023**, *56*, 2197–2212.
[9] J. D. Tovar, R. Leblay, Y. Wang, L. Wojcik, A. Thibon-Pourret, M. Réglier, A. J. Simaan, N. L. Poul, C. Belle, *Chem. Sci.* **2024**, *15*, 10308–10349.
[10] D. Diao, A. J. Simaan, A. Martinez, C. Colomban, *Chem. Commun.* **2023**, *59*, 4288–4299.
[11] S. D. McCann, S. S. Stahl, *Accounts Chem Res* **2015**, *48*, 1756–1766.
[12] P. Specht, A. Petrillo, J. Becker, S. Schindler, *Eur. J. Inorg. Chem.* **2021**, *2021*, 1961–1970.
[13] R. Leblay, R. Delgadillo-Ruíz, C. Decroos, C. Hureau, M. Réglier, I. Castillo, B. Faure, A. J. Simaan, *ChemCatChem* **2023**, *15*, e20230093, Doi: 10.1002/cctc.202300933.
[14] R. Trammell, K. Rajabimoghadam, I. Garcia-Bosch, *Chem. Rev.* **2019**, *119*, 2954–3031.
[15] T. Abe, Y. Hori, Y. Shiota, T. Ohta, Y. Morimoto, H. Sugimoto, T. Ogura, K. Yoshizawa, S. Itoh, *Commun. Chem.* **2019**, *2*, 12.
[16] B. Kim, D. Jeong, J. Cho, *Chem. Commun.* **2017**, *53*, 9328–9331.
[17] B. Kim, D. Jeong, T. Ohta, J. Cho, *Commun. Chem.* **2019**, *2*, 81.
[18] P. K. Hota, S. Panda, H. Phan, B. Kim, M. A. Siegler, K. D. Karlin, *J. Am. Chem. Soc.* **2024**, *146*, 23854–23871.
[19] M.-C. Kafentzi, M. Orio, M. Réglier, S. Yao, U. Kuhlmann, P. Hildebrandt, M. Driess, A. J. Simaan, K. Ray, *Dalton Trans.* **2016**, *45*, 15994–16000.
[20] S. Fukuzumi, K.-B. Cho, Y.-M. Lee, S. Hong, W. Nam, *Chem. Soc. Rev.* **2020**, *49*, 8988–9027.
[21] D. Jeong, J. S. Valentine, J. Cho, *Coord. Chem. Rev.* **2023**, *480*, 215021.
[22] U. K. Bagha, J. K. Satpathy, G. Mukherjee, C. V. Sastri, S. P. de Visser, *Org. Biomol. Chem.* **2020**, *19*, 1879–1899.
[23] R. Zhao, B.-B. Zhang, Z. Liu, G.-J. Cheng, Z.-X. Wang, *JACS Au* **2022**, *2*, 745–761.
[24] A. W. Addison, T. N. Rao, J. Reedijk, J. van Rijn, G. C. Verschoor, *J. Chem. Soc., Dalton Trans.* **1984**, 1349–8.
[25] C.-Y. Wu, C.-C. Su, *Polyhedron* **1997**, *16*, 383–392.
[26] F. Lebon, M. Ledecq, M. Dieu, C. Demazy, J. Remacle, R. Lapouyade, O. Kahn, F. Durant, *J. Inorg. Biochem.* **2001**, *86*, 547–554.
[27] I. Castro, J. Faus, M. Julve, J. M. Amigó, J. Sletten, T. Debaerdemaeker, *J. Chem. Soc. Dalton Trans.* **1990**, *0*, 891–897.
[28] L. Carlucci, G. Ciani, S. Maggini, D. M. Proserpio, R. Sessoli, F. Totti, *Inorg. Chim. Acta* **2011**, *376*, 538–548.
[29] L. H. Abdel-Rahman, M. T. Basha, B. S. Al-Farhan, M. R. Shehata, S. K. Mohamed, Y. Ramli, *J. Mol. Struct.* **2022**, *1247*, 131348.
[30] E. Garribba, G. Micera, *J. Chem. Educ.* **2006**, *83*, 1229.
[31] J. Peisach, W. E. Blumberg, *Arch. Biochem. Biophys.* **1974**, *165*, 691–708.
[32] U. Sakaguchi, A. W. Addison, *J. Chem. Soc., Dalton Trans.* **1979**, 600–9.
[33] W. Zhang, B. Zhang, Q. Sun, *Iucrdata* **2021**, *6*, x210672.
[34] H. Kooijman, A. L. Spek, D. Rehorst, W. L. Driessen, J. Reedijk, *Acta Crystallogr. Sect. C* **1997**, *53*, 1596–1598.
[35] C. Abolin, J. D. McRae, T. N. Tozer, S. Takki, *Biochem Med Metab B* **1980**, *23*, 209–218.
[36] A. D. Fraser, W. MacNeil, *J. Anal. Toxicol.* **1989**, *13*, 73–76.
[37] J. Chen, A. Draksharapu, D. Angelone, D. Unjaroen, S. K. Padamati, R. Hage, M. Swart, C. Duboc, W. R. Browne, *ACS Catal.* **2018**, *8*, 9665–9674.
[38] C. M. de Roo, A. Sardjan, R. Postmus, M. Swart, R. Hage, W. R. Browne, *ChemCatChem* **2024**, *16*, e202301594, Doi: 10.1002/cctc.202301594.
[39] E. M. Simmons, J. F. Hartwig, *Angew. Chem. Int. Ed.* **2012**, *51*, 3066–3072.
[40] K. B. Wiberg, *Chem. Rev.* **1955**, *55*, 713–743.
[41] M. Bonifačić, D. A. Armstrong, I. Štefanić, K.-D. Asmus, *J. Phys. Chem. B* **2003**, *107*, 7268–7276.
[42] Y. Manevich, K. D. Held, J. E. Biaglow, *Radiat. Res.* **1997**, *148*, 580.
[43] C. Cheignon, F. Collin, P. Faller, C. Hureau, *Dalton Trans.* **2016**, *45*, 12627–12631.
[44] R. A. Sheldon, I. W. C. E. Arends, G.-J. ten Brink, A. Dijksman, *Accounts Chem Res* **2002**, *35*, 774–781.
[45] B. Xu, J. Lumb, B. A. Arndtsen, *Angew. Chem. Int. Ed.* **2015**, *54*, 4208–4211.
[46] O. Das, T. K. Paine, *Dalton Trans.* **2012**, *41*, 11476–11481.
[47] M. F. Semmelhack, C. R. Schmid, D. A. Cortes, C. S. Chou, *J. Am. Chem. Soc.* **1984**, *106*, 3374–3376.
[48] D. Schäfer, F. Fink, D. Kleinschmidt, K. Keisers, F. Thomas, A. Hoffmann, A. Pich, S. Herres-Pawlis, *Chem. Commun.* **2020**, *56*, 5601–5604.
[49] S. D. McCann, S. S. Stahl, *Acc. Chem. Res.* **2015**, *48*, 1756–1766.
[50] B. L. Ryland, S. D. McCann, T. C. Brunold, S. S. Stahl, *J. Am. Chem. Soc.* **2014**, *136*, 12166–12173.
[51] J. M. Hoover, B. L. Ryland, S. S. Stahl, *J. Am. Chem. Soc.* **2013**, *135*, 2357–2367.
[52] S. E. Allen, R. R. Walvoord, R. Padilla-Salinas, M. C. Kozlowski, *Chem. Rev.* **2013**, *113*, 6234–6458.
[53] J. L. Jeffrey, J. A. Terrett, D. W. C. MacMillan, *Science* **2015**, *349*, 1532–1536.
[54] P. H. Taylor, T. Yamada, P. Marshall, *Int. J. Chem. Kinet.* **2006**, *38*, 489–495.
[55] S. S. Nag, G. Mukherjee, P. Barman, C. V. Sastri, *Inorg. Chim. Acta* **2019**, *485*, 80–85.

[56] P. Barman, P. Upadhyay, A. S. Faponle, J. Kumar, S. S. Nag, D. Kumar, C. V. Sastri, S. P. de Visser, *Angew. Chem.* **2016**, *128*, 11257–11261.
[57] G. da Silva, J. W. Bozzelli, *J. Phys. Chem. A* **2006**, *110*, 13058–13067.
[58] W. Supronowicz, I. A. Ignatyev, G. Lolli, A. Wolf, L. Zhao, L. Mleczko, *Green Chem.* **2015**, *17*, 2904–2911.
[59] B. Thijs, J. Rongé, J. A. Martens, *Green Chem.* **2022**, *24*, 2287–2295.
[60] J. Friedl, U. Stimming, *Electrochim. Acta* **2013**, *101*, 41–58.
[61] D. Sebastián, A. Serov, I. Matanovic, K. Artyushkova, P. Atanassov, A. S. Aricò, V. Baglio, *Nano Energy* **2017**, *34*, 195–204.
[62] Y. Zheng, X. Wan, X. Cheng, K. Cheng, Z. Dai, Z. Liu, *Catalysts* **2020**, *10*, 166.
[63] L. Yaqoob, T. Noor, N. Iqbal, *RSC Adv.* **2021**, *11*, 16768–16804.
[64] H. Zhu, W. He, C. Zhan, X. Li, Z. Guan, F. Guo, J. Yao, *Tetrahedron* **2011**, *67*, 8458–8464.
[65] O. V. Dolomanov, L. J. Bourhis, R. J. Gildea, J. A. K. Howard, H. Puschmann, *J. Appl. Crystallogr.* **2009**, *42*, 339–341.
[66] G. M. Sheldrick, *Acta Crystallogr. Sect. A* **2015**, *71*, 3–8.
[67] G. M. Sheldrick, *Acta Crystallogr C Struct Chem* **2015**, *71*, 3–8.
[68] S. Stoll, A. Schweiger, *J. Magn. Reson.* **2006**, *178*, 42–55.

Manuscript received: February 17, 2025
Accepted manuscript online: February 21, 2025
Version of record online: April 22, 2025